Metal Binding to *Saccharomyces cerevisiae* Ferrochelatase†

Tobias Karlberg,‡ David Lecerof,‡ Monika Gora,§ Germund Silvegren,‡ Rosine Labbe-Bois,|| Mats Hansson,⊥ and Salam Al-Karadaghi*,‡

Department of Molecular Biophysics and Department of Biochemistry, Centre for Chemistry and Chemical Engineering, Lund University, P.O. Box 124, SE-221 00 Lund, Sweden, Institute of Biochemistry and Biophysics, Polish Academy of Sciences, Pawinskiego 5A, 02-106 Warsaw, Poland, and Laboratoire de Biochimie des Porphyrines, Institut Jacques Monod, Université Paris VII, 2 place Jussieu, 75251 Paris, France

Received May 6, 2002; Revised Manuscript Received July 27, 2002

ABSTRACT: Ferrochelatase is the terminal enzyme in the heme biosynthetic pathway. It catalyzes the insertion of ferrous iron into protoporphyrin IX to produce protoheme IX. The crystal structures of ferrochelatase from *Saccharomyces cerevisiae* in free form, in complex with Co(II), a substrate metal ion, and in complex with two inhibitors, Cd(II) and Hg(I), are presented in this work. The enzyme is a homodimer, with clear asymmetry between the monomers with regard to the porphyrin binding cleft and the mode of metal binding. The Co(II) and Cd(II) complexes reveal the metal binding site which consists of the invariant amino acids H235, E314, and S275 and solvent molecules. The shortest distance to the metal reveals that amino acid H235 is the primary metal binding residue. A second site with bound Cd(II) was found close to the surface of the molecule, approximately 14 Å from H235, with E97, H317, and E326 participating in metal coordination. It is suggested that this site corresponds to the magnesium binding site in *Bacillus subtilis* ferrochelatase. The latter site is also located at the surface of the molecule and thought to be involved in initial metal binding and regulation.

Heme is one of the key prosthetic groups in living cells. The terminal enzyme in the heme biosynthesis pathway, ferrochelatase (protoheme ferrolyase, EC 4.99.1.1), catalyzes insertion of ferrous iron into protoporphyrin IX to produce protoheme IX. In at least one organism, *Bradyrhizobium japonicum*, ferrochelatase has been shown to play a key role in the regulation of heme synthesis through direct interaction with the iron response regulator protein (*1*). In eukaryotes, ferrochelatase has been found to be associated with the matrix side of the inner mitochondrial membrane, while in prokaryotes, it is found in the cytoplasm or associated with the cytoplasmic membrane (*2*). The eukaryotic enzyme is synthesized in the cytosol and subsequently imported into the mitochondria, where the mitochondrial target sequence is removed and the protein matures to full functionality. The human enzyme (*3*) and that from *Saccharomyces cerevisiae* (*4*) have been shown to be homodimeric. All mammalian ferrochelatases that have been studied, and even ferrochelatase from the yeast *Schizosaccharomyces pombe* and some bacteria, contain an iron−sulfur cluster ([2Fe-2S]) at the C-terminus (*5*, *6*). The function of the cluster is unknown. From studies of the human enzyme, however, the part of the structure to which it belongs is known to contribute to dimer stabilization (*3*).

X-ray crystallographic structures of *Bacillus subtilis* (*7*) and human ferrochelatase (*3*) have been determined. The molecules have a conserved overall fold of two Rossmann-type domains which together contribute to the formation of the porphyrin binding cleft. The differences between the structures are concentrated to the region in the human enzyme suggested to be involved in interactions with membranes and to the C-terminus, which contains the iron−sulfur cluster, which is absent in the *B. subtilis* enzyme. A fold similar to that of ferrochelatase has also been observed for *Salmonella typhimurium* anaerobic cobalt chelatase (Co chelatase), demonstrating a clear evolutionary relationship between these two enzymes (*8*). In contrast, the ATP-dependent Mg chelatase and its homologue, the aerobic Co chelatase, are composed of three subunits and are regulated by a chaperone-like AAA-type ATPase module (*9*, *10*).

According to the general reaction scheme, distortion of the porphyrin macrocycle is considered to be the first step in the mechanism of metalation. The steps following this include outer sphere complex formation, exchange of the coordinated solvent with the first pyrrolenine nitrogen (rate-determining), chelating ring closure to form the sitting-atop complex (SAT,[1] Figure 1), and a first deprotonation of the pyrrole nitrogen by a basic solvent, followed by a second deprotonation and metalloporphyrin formation (*11*). The way

† This work was supported by grants from the Swedish Research Council (to S.A.-K.) and the Swedish Research Council for Environment, Agricultural Sciences and Spatial Planning (to M.H.).

* To whom correspondence should be addressed: Department of Molecular Biophysics, Centre for Chemistry and Chemical Engineering, Lund University, P.O. Box 124, SE-221 00 Lund, Sweden. Telephone: +46 46 2224512. Fax: +46 46 2224692. E-mail: Salam.Al-Karadghi@mbfys.lu.se.

‡ Department of Molecular Biophysics, Centre for Chemistry and Chemical Engineering, Lund University.

§ Polish Academy of Sciences.

|| Université Paris VII.

⊥ Department of Biochemistry, Centre for Chemistry and Chemical Engineering, Lund University.

[1] Abbreviations: SAT, sitting-atop; *N*-MeMP, *N*-methylmesoporphyrin IX.

10.1021/bi0260785 CCC: $22.00
Published on Web 10/23/2002

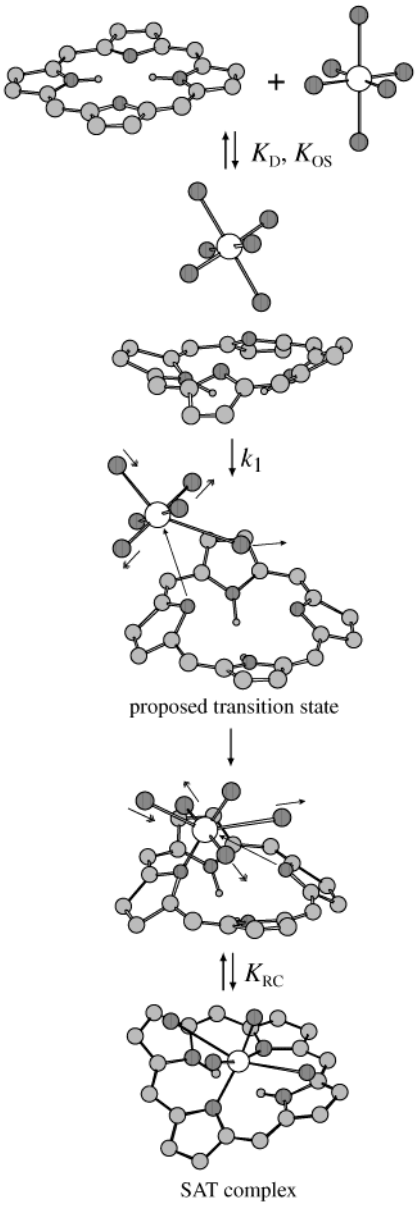

FIGURE 1: Schematic view of the formation of a SAT complex, prior to metal insertion into porphyrin. Adapted from ref *34* with permission.

the porphyrin is distorted and the nature of the distortion have been extensively studied recently. Thus, the structure of *B. subtilis* ferrochelatase in complex with the transition state analogue *N*-methylmesoporphyrin IX (*N*-MeMP) revealed the mode of porphyrin binding and suggested that the enzyme induces a distortion in the macrocycle by fixing pyrrole rings B−D and forcing ring A to tilt (*12*). Resonance Raman data have also demonstrated porphyrin distortion upon complex formation in ferrochetalase from both mouse and *S. cerevisiae* (*13*−*15*). However, for yeast ferrochelatase, the induced distortion could only be seen when mercury, a known inhibitor, was also bound (*13*). This led the authors to suggest an allosteric mechanism, according to which metal binding induces a conformational change in the protein which, in turn, forces a distortion on the porphyrin macrocycle.

An understanding of the details of the mechanism of catalytic porphyrin metalation requires that the position of the metal binding site and its relation to the bound porphyrin be revealed. Although it is currently accepted that the porphyrin binds in a cleft between the two domains of ferrochelatase, the location of the metal binding site, or sites, and the nature of the metal ligands are still being debated. Mutational studies on human and *S. cerevisiae* ferrochelatase have implicated an invariant histidine (H263 and H235, respectively) as being involved in substrate metal binding (*16*, *17*). Metal binding to the corresponding residue in *B. subtilis* ferrochelatase (H183) was directly observed by X-ray crystallography in metal soaking experiments (*7*). The structure of the complex with *N*-MeMP has also demonstrated that this histidine is located in the porphyrin binding cleft in the proximity of the distorted pyrrole ring (*12*). The involvement in metal binding of the corresponding residue in mouse ferrochelatase (H207) has recently been demonstrated using X-ray absorption spectroscopy (*18*). On the other hand, soaking the human ferrochelatase crystals with Co(II) showed metal binding at the side of the molecule opposite the porphyrin binding cleft, ~20 Å from H263 (*3*). This site has been suggested by the authors to be used for initial metal binding. At the second stage, the metal would travel through the core of the molecule to enter the macrocycle (*19*). The discrepancy between the results raises several questions. Is there an initial metal binding site from which the metal travels to enter the porphyrin, and if so, what would be the path of the metal?

In this work, we present the crystal structure of ferrochelatase from *S. cerevisiae* in free form, in complex with a substrate metal, Co(II), and in complex with two inhibitors, Cd(II) and Hg(I). The results show that in yeast, the invariant H235 is the primary metal binding residue. In addition, the invariant residues glutamate E314 and serine S275 and solvent molecules contribute to metal coordination.

MATERIALS AND METHODS

Crystallization and Data Collection. The pMG2 plasmid was constructed as described previously (*17*) to express the mature form of *S. cerevisiae* ferrochelatase under the *Escherichia coli* alkaline phosphatase promoter phoA as described by Ferreira (*20*). The plasmids were transformed into *E. coli* strain DH5α (Life Technologies, Inc.), and the bacteria were grown to saturation in LB/ampicillin medium, diluted 1:100 in complete low-phosphate/MOPS medium containing 100 mg/L ampicillin, and incubated for 18−20 h at 37 °C. The cells were harvested by centrifugation, resuspended in 0.1 M Tris-HCl buffer (pH 7.6) containing 20% glycerol and 10 μg/mL phenylmethanesulfonyl fluoride, and disrupted by sonication. The lysed cells were centrifuged (100000*g* for 1 h at 4 °C) to separate the membrane and soluble fractions. The membrane pellets were resuspended in the above buffer. All fractions were analyzed immediately or stored at −20 °C. Ferrochelatase activity was monitored spectroscopically by directly recording the rate of zinc protoporphyrin formation as described in detail previously (*21*), and by references therein. The protein was purified as described previously (*17*) and stored in 0.1 M Tris-HCl (pH 8.0), 20% (w/v) glycerol, and 1% (w/v) *N*-octyl β-D-glucopyranoside. Crystals were grown by vapor diffusion in a hanging drop at 4 °C. Crystallization drops were made by mixing 5 μL of a protein solution with 5 μL of a reservoir solution containing 0.1 M Tris-HCl (pH 7.5), 23% (w/v) PEG2000, and 10% (v/v) 2-propanol. One microliter of 1-*S*-

Table 1: Details of Data Collection and Refinement Statistics for *S. cerevisiae* Ferrochelatase

	native enzyme	Co(II)-soaked	Hg(II)-soaked	Cd(II)-soaked
data collection				
cell dimensions *a*, *b*, *c* (Å)[a]	86.6, 97.2, 121.6	84.4, 96.7, 120.7	84.7, 96.5, 120.7	84.5, 95.6, 119.8
resolution range (Å)	10−2.4	15−2.7	20−3.4	20−3.7
completeness (%)	92.5	90.9	77.7	87.1
no. of unique reflections	37088	22973	20437	18665
$I/\sigma(I) > 3$ (%)	77.2	67.6	55.1	85.3
R_{merge} (%)[b]	10.5	17.4	9.8	8.6
in the highest-resolution shell				
resolution range (Å)	2.5−2.4	2.9−2.7	3.5−3.4	4.0−3.7
completeness (%)	80.9	60.9	48.4	61.5
$I/\sigma(I) > 3$ (%)	33.0	22.9	19.6	68.8
R_{merge} (%)[b]	19.9	30.2	24.3	20.5
refinement				
no. of protein atoms	5677	5666		
no. of water molecules	122	10		
R_{cryst} (R_{free})[c] (%)	25.5 (28.2)	23.7 (28.7)		
rmsd[d]				
bond lengths (Å)	0.007	0.010		
bond angles (deg)	1.6	1.8		
dihedrals (deg)	22.7	22.8		
average *B*-factor (Å^2)	45.3	47.7		

[a] Space group $P2_12_12_1$. [b] $R_{merge} = \sum|I_i - \langle I\rangle|/\sum I$, where I_i is an individual intensity measurement and $\langle I\rangle$ is the average intensity for this reflection. [c] $R_{cryst} = \sum|F_{obs} - F_{calc}|/\sum F_{obs}$, where F_{obs} and F_{calc} are the observed and calculated structure factor amplitudes, respectively. R_{free} is the same as R_{cryst}, but calculated on 5% of the data excluded from refinement. [d] Root-mean-square deviations of the parameters from their ideal values.

octyl β-D-thioglucoside (Hampton detergent screen) was added to the drops. Crystals appeared after 5−7 weeks. The best crystals had dimensions of approximately 0.6 mm × 0.5 mm × 0.5 mm. For data collection, crystals were mounted on a rayon loop and flash-cooled directly in a stream of boiled-off nitrogen. Data to 2.4 Å resolution were collected using a MAR Research CCD detector at MAX II synchrotron laboratory station BL711 in Lund (*22*), and processed with the XDS package (*23*). The space group is $P2_12_12_1$ with the following unit cell parameters: $a = 86.6$ Å, $b = 97.2$ Å, and $c = 121.6$ Å.

Metals were soaked into the native crystals at a concentration of ~0.6 mM for 6, 48, and 2.5 h for $CdCl_2$, $HgCl_2$, and $CoCl_2$, respectively. For soaking, the crystals were transferred from their original drops to a 20 μL drop of the reservoir solution to which the heavy metal solution was added. Addition of detergent to these drops was not required. Data were collected to resolutions of 3.7, 3.4, and 2.7 Å for $CdCl_2$, $HgCl_2$, and $CoCl_2$, respectively.

Refinement and Model Building. The data were divided into a working set (95%) and a test set (5%) that was used to monitor R_{free} (*24*). The structure was determined by the method of molecular replacement, using the model of human ferrochelatase [PDB entry 1HRK (*3*)]. After rigid-body refinement and density modification using the CNS package (*25*), an interpretable Fourier map was calculated. The main chain was first fitted into the density, and then the side chains were replaced when needed and rebuilt using the program O (*26*). After several cycles of refinement, the model converged to an R_{cryst} of 25.5% ($R_{free} = 28.2\%$). Kleywegt et al. (personal communication) have calculated expected values of R_{free} for a given resolution on a set of 6500 PDB entries. At 2.4 Å, 90% of the structures had an R_{free} value between 22 and 30%. Hence, the R_{free} that was obtained is within the normal range. The final model consists of 710 amino acid residues (98% complete) and 122 water molecules. In one of the monomers, subunit B, some electron density of a detergent, or a lipid molecule is seen within the active site pocket. It is, however, rather weak and does not allow any reliable identification. This density is only present in the native protein and not in any of the metal-soaked complexes. The Ramachandran plot (*27*) of the main chain torsion angles (ϕ and ψ) shows that 86.0% of the residues are in the most favored regions as defined in the program PROCHECK (*28*). The refined model was used for additional refinement of the complex with Co(II). The final R_{cryst} for this model was 23.7% (28.7%). Data collection and refinement statistics are presented in Table 1. The coordinates have been deposited in the Protein Data Bank [entry 1LBQ for the native protein and entry 1L8X for the Co(II)-soaked complex].

RESULTS

Overall Structure. S. cerevisiae ferrochelatase is expressed in the nucleus and transported into the mitochondrion. A higher-molecular mass precursor (monomeric mass of 44 kDa) rapidly matures in vivo (*29*), resulting in a polypeptide of 362 amino acid residues (residues 32−393). Residues 1−31 constitute the mitochondrial target sequence. The model presented in this work is a homodimer and contains residues 36−391 and 38−391 in the first and second monomers, respectively (Figure 2A). It confirms earlier biochemical experiments (*4*) which demonstrated that the functional protein is a homodimer. The size of the monomer is approximately 65 Å × 45 Å × 40 Å, and it contains 14.3% β-sheet and 47.7% helix. Similar to the ferrochelatase structures of *B. subtilis* (*7*) and *Homo sapiens* (*3*), the monomer has two similar domains, each folded into a Rossmann-type fold with a four-stranded parallel β-sheet flanked by α-helices on both sides. The connectivity between the domains consists of a loop and a helical turn (residues 218−227). Using the convention that has been adopted, the first domain consists of α-helices 1−6 and β-strands 1−4 while the second domain is built up from α-helices 7−13 and β-strands 5−8. Helix 10 contains a π-helix, present in

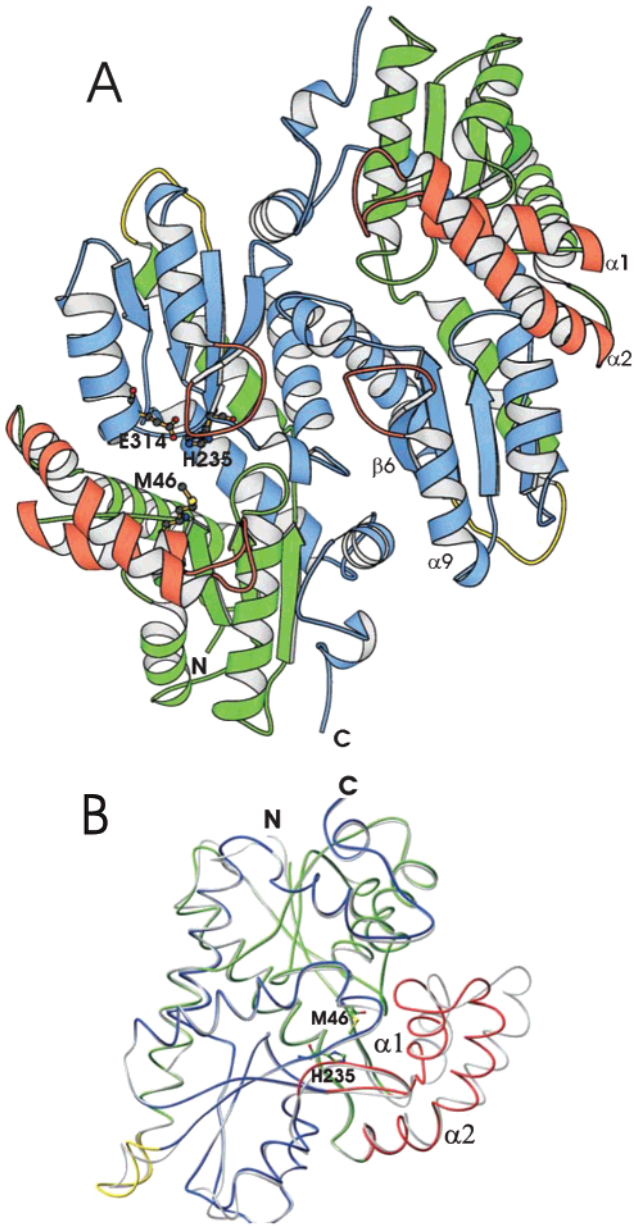

FIGURE 2: (A) Ribbon presentation of the three-dimensional structure of *S. cerevisiae* ferrochelatase. N and C mark the N- and C-termini, respectively. The residues on the two sides of the porphyrin binding cleft (H235, E314, and M46) are shown as a ball-and-stick model. The linker region between the domains is shown in yellow, while regions involved in building up the porphyrin binding cleft (helices α1 and α2 and the loop between strand *β*6 and helix α9) are shown in red. (B) Least-squares superposition of the two monomers showing different conformations in the region of helices 1 and 2 and the loop between them (shown in red). One of the monomers is colored gray, while for the other, the color scheme of panel A is preserved. This figure was prepared with the programs MOLSCRIPT (*35*) and RIBBONS (*36*).

all ferrochelatase structures and in the anaerobic Co chelatase structure (*30*).

A superposition of the two monomers shows that the largest difference between the structures is in the conformation of the region of helices 1 and 2 and the loop between them (residues 54−99, Figure 2B). The largest shifts in Cα atom positions are in the loop region, reaching around 8 Å. This region builds up part of the porphyrin binding cleft, and the difference in conformation results in a considerably more open porphyrin binding cleft in one of the monomers (monomer A), when compared to the other (monomer B). It is unclear whether this difference is due to interactions of the loop between helices 1 and 2 (residues 65−75) with a symmetry-related molecule within the crystal lattice or if there is true asymmetry between the subunits. The more open conformation of monomer A is very similar to the conformation of the same region in *B. subtilis* ferrochelatase in complex with *N*-MeMP. A superposition with this structure also shows that the bent conformation of the loop in monomer B results in residues 67−71 occupying a position where the porphyrin molecule is expected to bind. As shown later, the asymmetry between the monomers is also preserved when metal binding is considered.

The loop of residues 65−75 includes several exposed hydrophobic residues, L68, I69, P70, and I71. Opposite this region is another loop from the second domain (residues 272−285), which also includes several exposed hydrophobic residues, V277, G278, P279, P281, W282, L283, G284, and A285. These regions also have a hydrophobic character in the human ferrochelatase. The presence of positively charged residues (K74 and K280 in yeast) at the periphery of the hydrophobic region strongly suggests that it is involved in interactions with lipid membranes. Earlier results have also shown that ferrochelatase from *S. cerevisiae* requires fatty acids to be active (*29*), and residues within the lips, which surround the porphyrin binding cleft, have been suggested to be involved in membrane association (*31*). Thus, the structure confirms that at least part of the entrance to the active site should be facing the lipid membrane. Several additional patches of positively charged residues can be seen on the surface of the molecule (Figure 3). The residues which contribute to the formation of the patches are K74, K77, K81, K85, R87, K90, K93, and K280.

Dimer Stabilization and Comparison with Other Structures. The interface between the monomers is built up by parts of helices α7, α8, and α12, strand *β*6, and part of the loop between strand *β*6 and helix α9. The residues in these regions form an extensive hydrophobic core and contribute main chain and side chain hydrogen bonds (G245, F265, N267, Y269, R270, G284, N365, Q366, and D370) to dimer stabilization. Essentially the same interactions stabilize the monomers in the human enzyme. Hydrogen bonding interactions are contributed by N271, G273, Q278, Q285, Y297, R298, G312, R325, R327, T400, P404, and C406 (human numbering). The majority of these residues are conserved in eukaryotic ferrochelatase sequences (Figure 4). Helices α7 and α8 and the loop between strand *β*6 and helix α9 are all in the proximity of the porphyrin binding cleft. Apart from the destabilization of the dimer interface, distortions of the interactions within this region may affect the porphyrin binding cleft and, presumably, the catalytic activity of the enzyme. Thus, truncation mutants of *S. cerevisiae* lacking either the last 16 or 37 residues have no enzyme activity (*32*). Another result of the truncations would be elimination of the interactions of the loop between helices α12 and α13 with the loop between helices α1 and α2. As mentioned above, helices α1 and α2 and the loop between them constitute part of the porphyrin binding cleft. The interactions within this region may control the stability of the porphyrin binding cleft and serve in signal transduction between the cleft and the C-terminal part of the structure. Similar

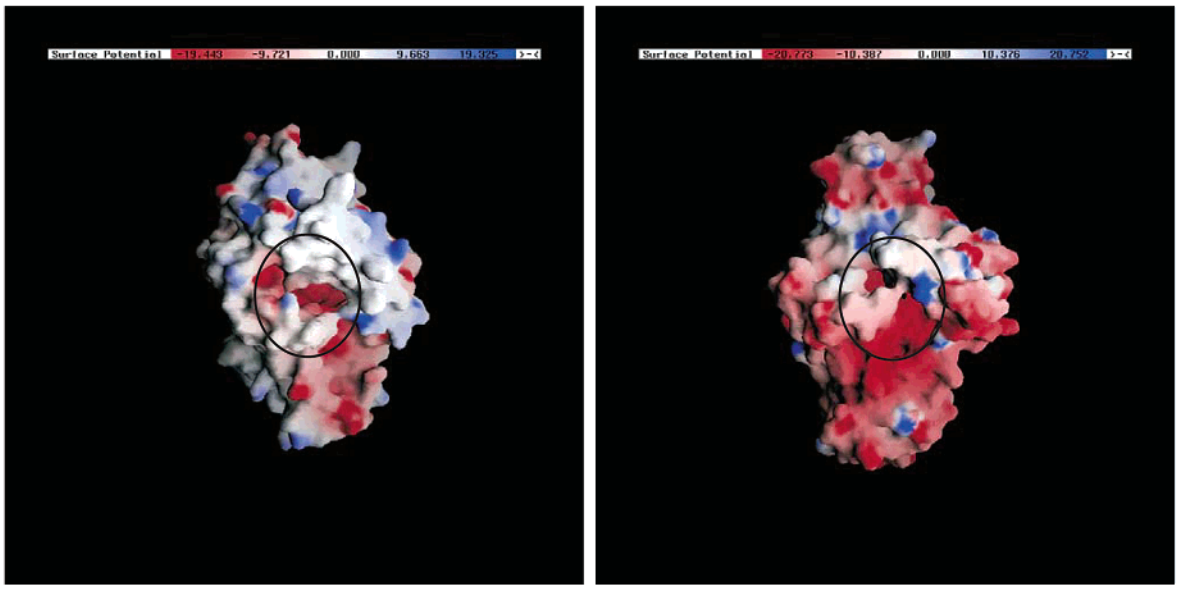

FIGURE 3: Electrostatic surface potentials of *S. cerevisiae* (left) and *B. subtilis* (right) ferrochelatases. The orientation of the molecules is similar to that of Figure 2A. The porphyrin binding cleft is highlighted with a circle. This figure was prepared using GRASP (*37*).

interactions are present in the human enzyme, although in this case the loop between helices α1 and α2 is two residues shorter.

Superimposition of one of the monomers of the yeast enzyme with the *B. subtilis* and the human enzyme structures gave rms deviations of 1.72 and 0.89 Å for the Cα atoms of 254 and 308 aligned residues, respectively. The major differences between the human and yeast enzymes are in the C-terminal part, which has different secondary structure in the two molecules. Thus, instead of helix α12 in yeast, there is a coil in the human enzyme, while helix α13 of the human structure is substituted with a coil in yeast (Figure 5). Interestingly, the C-terminus of the human enzyme could be replaced with the C-terminus of *S. cerevisiae*, with preservation of enzyme activity. However, if in the same mutant the last 10 amino acid residues (of the yeast sequence) are replaced with the human sequence, the enzyme becomes inactive (*32*). Thus, the absence of the [2Fe-2S] cluster in yeast does not seem to affect dimer stabilization, and presumably not the interactions between the C-terminus and the loop between helices α1 and α2, which was mentioned above.

Comparison of the three-dimensional structures of the *N*-MeMP complex of *B. subtilis* ferrochelatase with *S. cerevisiae* ferrochelatase shows a high level of conservation of the porphyrin binding pocket. The conserved residues on one side of the porphyrin ring (A182, H183, S184, L185, P186, and M187 by *B. subtilis* ferrochelatase numbering) can be superimposed on the corresponding residues of the yeast structure (A234, H235, S236, L237, P238, and M239) with a root-mean-square deviation of 0.53 Å for the Cα atoms. As mentioned above, the cleft in monomer A of the yeast structure has an open conformation resembling the conformation of the *N*-MeMP complex of the *B. subtilis* enzyme (*12*). On the other hand, the cleft in the two monomers of the human enzyme has a closed conformation, similar to the structure of the *B. subtilis* enzyme without inhibitor. It can be concluded that the presence of three detergent molecules in the porphyrin binding cleft of the human enzyme did not trigger a more open conformation.

Metal Binding. Co(II) is among the metals which can serve as a substrate for the ferrochelatase reaction. X-ray data collected from *S. cerevisiae* crystals soaked with Co(II) clearly show high difference electron density for the metal in the porphyrin binding cleft. However, there is a difference in the way the metal is bound in each of the monomers. Thus, in monomer A, the metal is bound to the invariant H235 at a distance of 2.0 Å. In addition, three solvent molecules are weakly coordinated to the metal at distances of 4.4, 3.4, and 3.6 Å; the last one even makes a bridge to E314 at a distance of 3.5 Å (Figure 6A). In monomer B, the metal is coordinated to H235 and E314 at distances of 1.9 and 2.8 Å, respectively, and weakly to the side chain of S275 (3.7 Å) and a water molecule (4.2 Å) (Figure 6B). It should be noted that this is the first time we could observe the interaction of S275 with a metal. This residue is invariant in all ferrochelatase sequences, and its function is unclear. Metal coordination in both monomers resembles a distorted tetrahedral coordination, although the distances to the ligands, with the exception of H235, are too long for normal metal−ligand coordination. The distance between the Co ions, when the monomers are superimposed, is ∼2 Å, the metal in monomer A being closer to the surface of the molecule. A superposition of the metal complex with the metal-free structure shows that the positions of the protein side chains around the metal are largely preserved in monomer A. In monomer B, the side chain of E314 is shifted by ∼1.9 Å while the side chain of S275 has rotated to a position closer to the metal. The reason for the differences in metal coordination in the two monomers is not clear. One possibility could be that the more closed cleft of subunit B contributes to the stabilization of binding of the metal at a position where it may coordinate E314.

Among known inhibitors of ferrochelatase are the heavy metals cadmium and mercury (*33*). Examination of electron density maps calculated using data collected from crystals soaked with Cd^{2+} shows that two Cd^{2+} ions bind to each subunit (Figure 6C). One of the metals is bound to a site similar to that of the cobalt. In monomer A it is coordinated by H235 and S275 (at 2.8 and 3.3 Å, respectively) and in monomer B by H235, S275, and E314 (at 2.8, 3.7, and 2.3

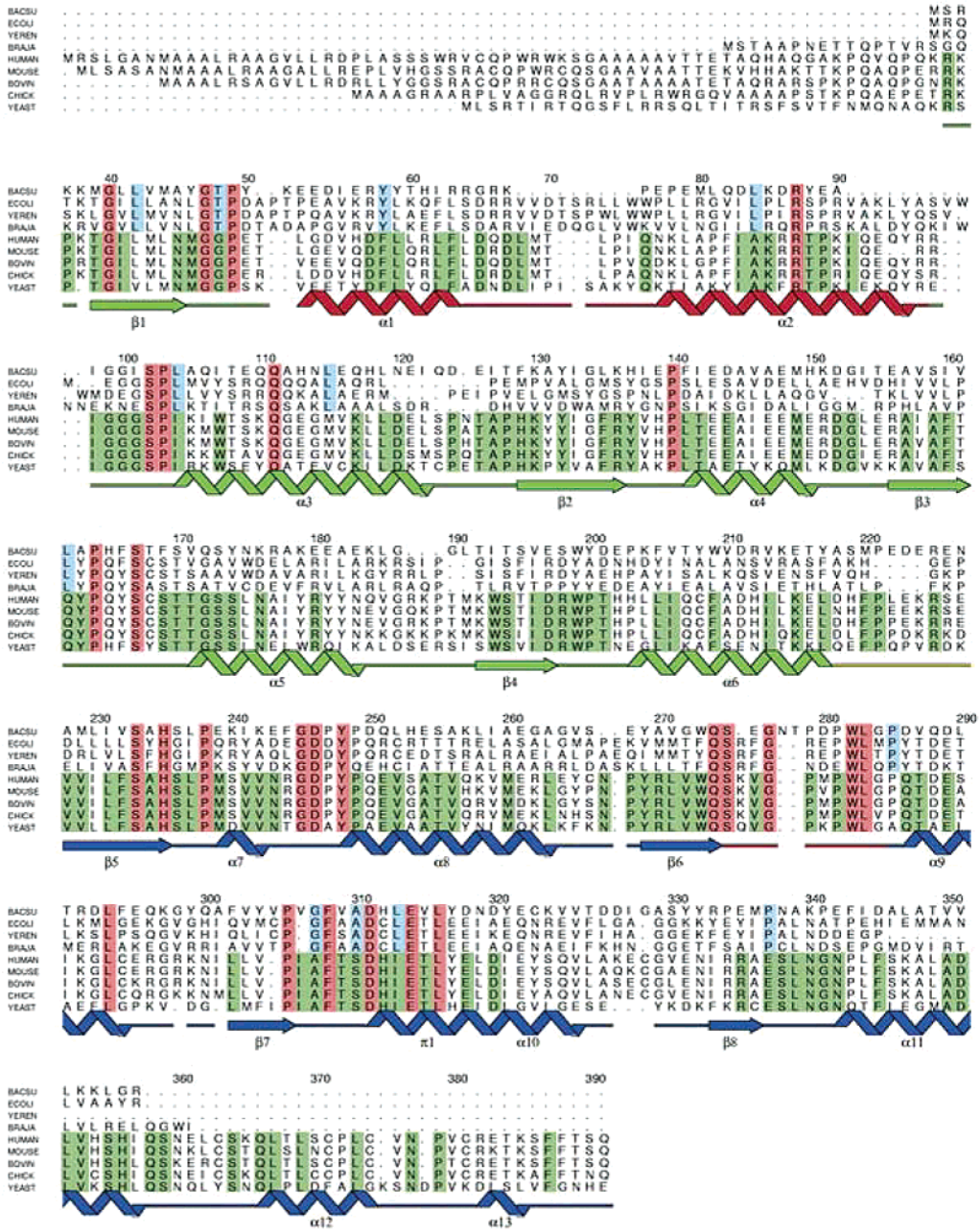

FIGURE 4: Structure-based alignment of ferrochelatase sequences. Colored boxes highlight conserved residues: red for residues in all sequences and blue and green for residues in bacteria and eukaryotes, respectively. Secondary structure elements of *S. cerevisiae* ferrochelatase are shown under the alignment. As in Figure 2A, green and blue refer to domains 1 and 2, respectively, and red refers to structural elements that build up the porphyrin binding cleft. Abbreviations: BACSU, *B. subtilis*; ECOLI, *E. coli*; YEREN, *Yersinia enterocolitica*; BRAJA, *Br. japonicum*. This figure was generated using ALSCRIPT (*38*).

Å, respectively). Thus, like Co(II), Cd(II) seems to bind in a different way to monomers A and B with the shortest distance of the metal to a ligand being that to the histidine. Although one should keep in mind that the resolution of the Cd data is low, which makes the positions of the side chains and the distances from the metal to its ligands less certain. The other Cd ion is coordinated by E97 and H317 (at approximately 2.4 and 2.7 Å in monomer A and 2.8 and 3.0 Å in monomer B, respectively). E326, which is ~5 Å from the metal, may also participate in the coordination, most probably through a solvent molecule, although solvent is not visible at this resolution. This site is located approximately 14 Å from H235 and 10 Å from E314. The low resolution of the data does not allow a reliable refinement of the model, or of the occupancy of the metals. An examination of the difference electron density maps shows that the density for both metals in monomer A can be seen up to a σ level of 9. In monomer B, the electron density for the metal at H235 and H317 remains up to σ levels of 12 and 7, respectively. This indicates that in both cases the occupancy of the metal is rather high.

The sequence alignment shows that the residues corresponding to E97 and E326 of *S. cerevisiae* in all other eukaryotic sequences are conserved as arginine and valine, respectively (Figure 4). It seems unlikely that such an "odd" substitution in yeast would occur by chance. Interestingly, one of the residues which was found to coordinate a magnesium ion in the *B. subtilis* structure, namely, E272

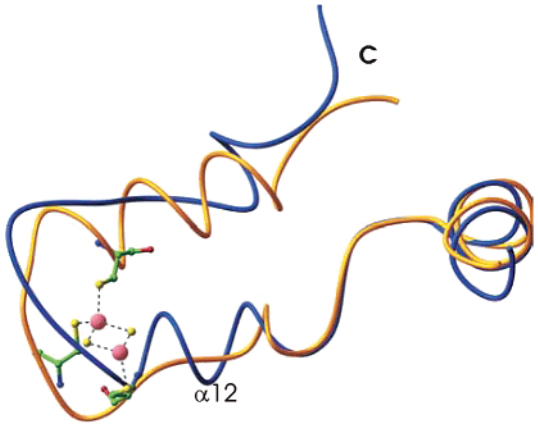

FIGURE 5: Superposition of the structures of yeast (blue) and human (yellow) ferrochelatase showing the difference in secondary structures at their C-terminal parts. The iron−sulfur cluster of the human enzyme is also shown (Fe as pink spheres and sulfur as yellow). This figure was prepared with RIBBONS (*36*).

(*B. subtilis* numbering), is conserved as a glutamate in most eukaryotic sequences but is replaced with a glycine (G322) in *S. cerevisiae*. This replacement will apparently abolish the ability of the molecule to bind metal at this site, which prompts us to suggest that the second Cd-binding site may have the same function as the magnesium site in the *B. subtilis* enzyme. However, since the distance between the two Cd-binding sites in this case is longer than the distance from the magnesium ion to H183 in *B. subtilis* (H235 in yeast), the interactions between them will be weaker.

Crystals soaked with mercury(II) diffracted to 3.4 Å. The difference electron density map revealed three Hg^{2+} atoms in the vicinity of C116, C123, and C336 in each monomer. None of these cysteine residues is conserved. All of the observed sites of Hg binding are located a rather long distance from the porphyrin binding cleft. This leaves unanswered the question of how the binding of this metal could result in deformation of the porphyrin macrocycle observed by Blackwood et al. (*13*).

DISCUSSION

In this work, we present the X-ray structure of *S. cerevisiae* ferrochelatase and its complexes with three different metals, one of which is known as a substrate (Co) and two of which are known as inhibitors (Cd and Hg). The overall fold of the molecule, when compared to the structures of *B. subtilis* and human ferrochelatase, is essentially preserved. Differences occur at the C-terminus, which in contrast to the human enzyme does not contain a [2Fe-2S] cluster, and in the region between helices 1 and 2. The residues involved in metal binding, H235 and E314, correspond to *B. subtilis* ferroche-

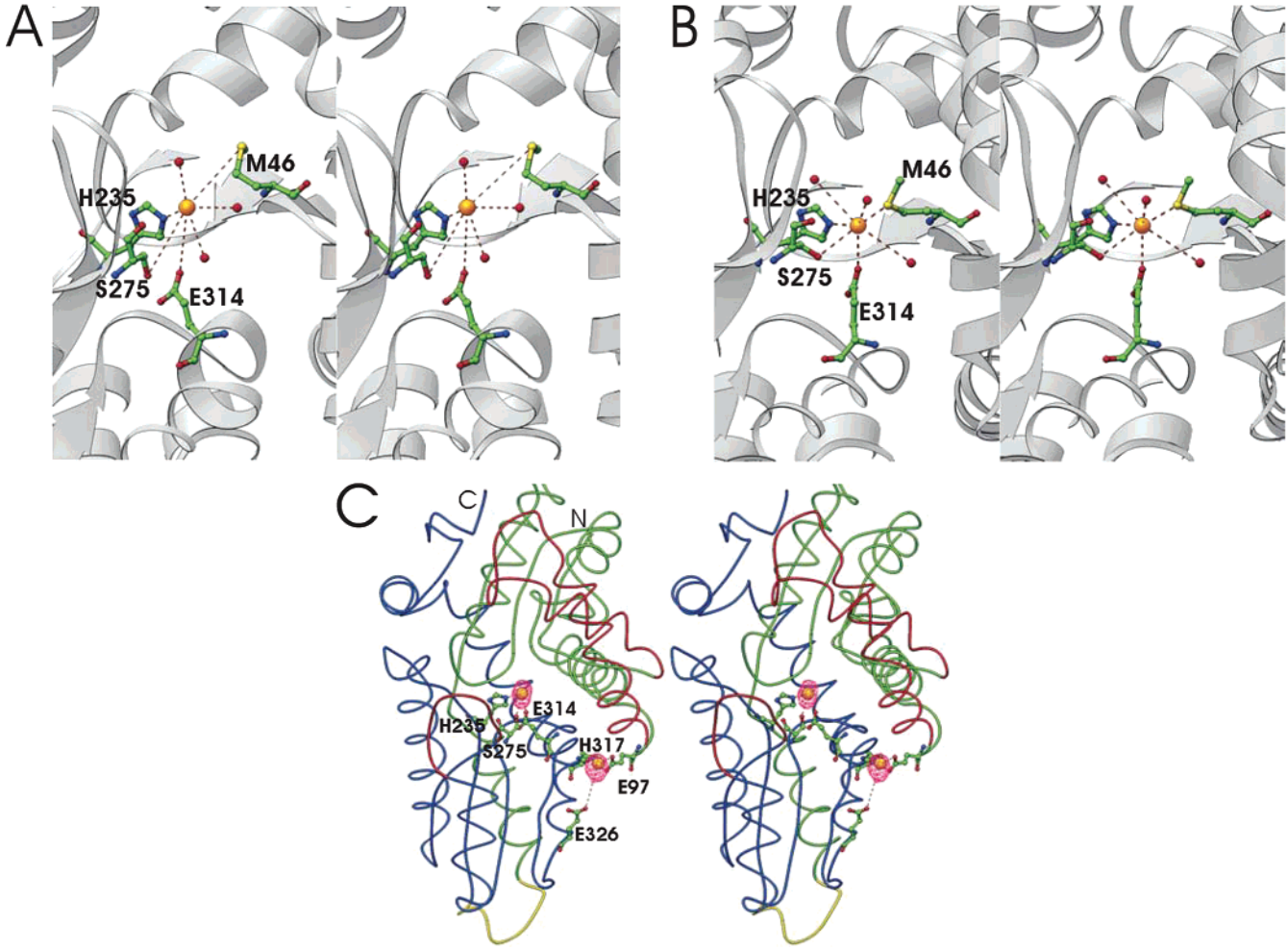

FIGURE 6: (A) Co(II) coordination in the active site of monomer A. (B) Co(II) coordination in the active site of monomer B. (C) Position of two Cd(II) ions. The difference electron density for Cd(II) is shown at the 5σ level. The metals and solvent are shown as orange and red spheres, respectively, and protein side chains (ball-and-stick model) which are involved in metal coordination are marked. This figure was generated using RIBBONS (*36*).

latase H183 and E264, respectively. H183 has been observed earlier to be involved in Cd(II) binding (*7*), while Zn(II) has been observed to coordinate both H183 and E264 (unpublished data). Recent X-ray absorption data and earlier biochemical studies have also shown that this invariant histidine is involved in metal binding in *S. cerevisiae*, mouse, and human ferrochelatase (*16*−*18*). In addition, Cd binds to a second site, which presumably has the same function as the Mg-binding site in the *B. subtilis* enzyme. Mercury binds to only cysteine residues. No indication of a metal bound to a site corresponding to that described for the human enzyme has been found in any of our soaking experiments. The residues proposed by Wu et al. (*3*) to initially bind metal in the case of human ferrochelatase, H230 and D383 (human ferrochelatase numbering), correspond to *S. cerevisiae* N202 and D350, respectively. N202 is located in a loop between strand β4 and helix α6, while D350 is located in the middle of helix α11. The distance from this site to the invariant H−E couple is approximately 20 Å. It should also be noted that, since the porphyrin binding cleft in the human ferrochelatase structure is occupied by three detergent molecules, the metal would first have to displace those to be able to bind to the site described in this work.

The short distances from Co(II) and Cd(II) to H235, when compared to the distances from other ligands, reveal this histidine to be the primary metal binding residue. The distances to the other ligands are too long for normal metal−ligand coordination, and they are much longer than the distances which were observed in X-ray absorption experiments for Co(II) binding to *S. cerevisiae* ferrochelatase (*18*). This discrepancy remains to be explained; however, the type of ligands suggested by the authors of this work largely agrees with the metal ligands found in our complexes.

The location of the site from which the metal enters the porphyrin is apparently crucial for understanding the reaction mechanism; its position is closely related to the mode of porphyrin distortion. The high level of conservation of the porphyrin binding cleft in the three ferrochelatases allows us to suggest that the mode of porphyrin binding and distortion are similar for these enzymes. If this is assumed, the positions of H235, E314, and S275 in relation to the position of the porphyrin, and particularly its distorted pyrrole ring, can be deduced from the three-dimensional structure of the complex of *N*-MeMP with *B. subtilis* ferrochelatase. In this structure, only one *N*-MeMP isomer (out of eight), which had its ring A tilted out of the plane of the porphyrin toward the conserved H−E couple (H183 and E264 in *B. subtilis*), was bound to the protein. Thus, the SAT metal−porphyrin complex (ref *34* and Figure 1) will most probably involve the pyrrolenine nitrogen of ring A, the invariant H235, and possibly E314 and S275. Sellers et al. (*19*) have, however, proposed that the invariant H−E couple is primarily involved in proton abstraction, while the metal will enter the macrocycle from the side of the ring which is opposite the side suggested by us. This would require a different mode of porphyrin distortion for a SAT complex to be formed.

REFERENCES

1. Qi, Z., and O'Brian, M. R. (2002) *Mol. Cell 9*, 155−162.
2. Dailey, H. A., Dailey, T. A., Wu, C. K., Medlock, A. E., Wang, K. F., Rose, J. P., and Wang, B. C. (2000) *Cell. Mol. Life Sci. 57*, 1909−1926.
3. Wu, C. K., Dailey, H. A., Rose, J. P., Burden, A., Sellers, V. M., and Wang, B. C. (2001) *Nat. Struct. Biol. 8*, 156−160.
4. Grzybowska, E., Gora, M., Plochocka, D., and Rytka, J. (2002) *Arch. Biochem. Biophys. 398*, 170−178.
5. Ferreira, G. C., Franco, R., Lloyd, S. G., Pereira, A. S., Moura, I., Moura, J. J., and Huynh, B. H. (1994) *J. Biol. Chem. 269*, 7062−7065.
6. Dailey, T. A., and Dailey, H. A. (2002) *J. Bacteriol. 184*, 2460−2464.
7. Al-Karadaghi, S., Hansson, M., Nikonov, S., Jonsson, B., and Hederstedt, L. (1997) *Structure 5*, 1501−1510.
8. Schubert, H. L., Raux, E., Wilson, K. S., and Warren, M. J. (1999) *Biochemistry 38*, 10660−10669.
9. Raux, E., Schubert, H. L., and Warren, M. J. (2000) *Cell. Mol. Life Sci. 57*, 1880−1893.
10. Fodje, M. N., Hansson, A., Hansson, M., Olsen, J. G., Gough, S., Willows, R. D., and Al-Karadaghi, S. (2001) *J. Mol. Biol. 311*, 111−122.
11. Lavallee, D. K. (1985) *Coord. Chem. Rev. 61*, 55−96.
12. Lecerof, D., Fodje, M., Hansson, A., Hansson, M., and Al-Karadaghi, S. (2000) *J. Mol. Biol. 297*, 221−232.
13. Blackwood, M. E., Jr., Rush, T. S., III, Romesberg, F., Schultz, P. G., and Spiro, T. G. (1998) *Biochemistry 37*, 779−782.
14. Franco, R., Ma, J. G., Lu, Y., Ferreira, G. C., and Shelnutt, J. A. (2000) *Biochemistry 39*, 2517−2529.
15. Lu, Y., Sousa, A., Franco, R., Mangravita, A., Ferreira, G. C., Moura, I., and Shelnutt, J. A. (2002) *Biochemistry 41*, 8253−8262.
16. Kohno, H., Okuda, M., Furukawa, T., Tokunaga, R., and Taketani, S. (1994) *Biochim. Biophys. Acta 1209*, 95−100.
17. Gora, M., Grzybowska, E., Rytka, J., and Labbe-Bois, R. (1996) *J. Biol. Chem. 271*, 11810−11816.
18. Ferreira, G. C., Franco, R., Mangravita, A., and George, G. N. (2002) *Biochemistry 41*, 4809−4818.
19. Sellers, V. M., Wu, C. K., Dailey, T. A., and Dailey, H. A. (2001) *Biochemistry 40*, 9821−9827.
20. Ferreira, G. C. (1994) *J. Biol. Chem. 269*, 4396−4400.
21. Labbe-Bois, R., and Camadro, J. M. (1994) in *Metal Ions in Fungi* (Winkelmann, G., and Winge, D. R., Eds.) pp 413−453, Dekker, New York.
22. Cerenius, Y., Ståhl, K., Svensson, L. A., Ursby, T., Oskarsson, Å., Albertsson, J., and Liljas, A. (2000) *J. Synchrotron Radiat. 7*, 203−208.
23. Kabsch, W. (1993) *J. Appl. Crystallogr. 26*, 795−800.
24. Brunger, A. T. (1992) *Nature 355*, 472−475.
25. Brunger, A. T., Adams, P. D., Clore, G. M., DeLano, W. L., Gros, P., Grosse-Kunstleve, R. W., Jiang, J. S., Kuszewski, J., Nilges, M., Pannu, N. S., Read, R. J., Rice, L. M., Simonson, T., and Warren, G. L. (1998) *Acta Crystallogr. D54*, 905−921.
26. Jones, T. A., Zou, J. Y., Cowan, S. W., and Kjeldgaard, M. (1991) *Acta Crystallogr. A47*, 110−119.
27. Ramachandran, G. N., and Sasisekharan, V. (1968) *Adv. Protein Chem. 23*, 283−438.
28. Laskowski, R. A., MacArthur, M. W., Moss, D. S., and Thornton, J. M. (1993) *J. Appl. Crystallogr. 26*, 283−291.
29. Camadro, J. M., and Labbe, P. (1988) *J. Biol. Chem. 263*, 11675−11682.
30. Fodje, M., and Al-Karadaghi, S. (2002) *Protein Eng. 15*, 353−358.
31. Gora, M., Rytka, J., and Labbe-Bois, R. (1999) *Arch. Biochem. Biophys. 361*, 231−240.
32. Medlock, A. E., and Dailey, H. A. (2000) *Biochemistry 39*, 7461−7467.
33. Dailey, H. A. (1987) *Ann. N.Y. Acad. Sci. 514*, 81−86.
34. Inamo, M., Kamiya, N., Inada, Y., Nomura, M., and Funahashi, S. (2001) *Inorg. Chem. 40*, 5636−5644.
35. Kraulis, P. (1991) *J. Appl. Crystallogr. 24*, 946−950.
36. Carson, M. (1991) *J. Appl. Crystallogr. 24*, 958−961.
37. Nicholls, A., Sharp, K. A., and Honig, B. (1991) *Proteins 11*, 281−296.
38. Barton, G. J. (1993) *Protein Eng. 6*, 37−40.

BI0260785